

Sensing of magnetic fields from biological signals using diamond nitrogen vacancy centres

April 7, 2020

James L. Webb^{1,*}, Luca Troise¹, Nikolaj W. Hansen², Jocelyn Achard³, Ovidiu Brinza³, Robert Staacke⁴, Michael Kieschnick⁴, Jan Meijer⁴, Jean-François Perrier², Kirstine Berg Sørensen¹, Alexander Huck¹ and Ulrik Lund Andersen¹

Abstract

1

Sensing of signals from biological processes such as action potential propagation in nerves, are essential for clinical diagnosis and basic understanding of physiology. Sensing can be performed electrically by placing sensor probes near or inside a living specimen, or on dissected tissue using well established electrophysiology techniques. However, these electrical probe techniques have poor spatial resolution and cannot easily access tissue deep within a living subject, in particular within the brain. An alternative approach is to read the magnetic field induced by the passage of the electrical signal, giving the equivalent readout without direct electrical contact. Such measurements are performed today using bulky and expensive superconducting sensors with poor spatial resolution. An alternative is to use nitrogen vacancy centres in diamond, that promise biocompatible high field sensitivity without cryogenic cooling. Here we discuss the challenges with this method in application to biosensing with reference to our own recent work and the wider field.

2 Introduction

Many biological processes generate electrical signals, for example synaptic transmission and muscular contraction. Such signals give key information on the functioning on biological systems, either for clinical diagnostic purposes (such as electrocardiography) or for fundamental understanding of processes and structure. Measuring these signals is typically performed using electrical probes carefully positioned in the desired region. This

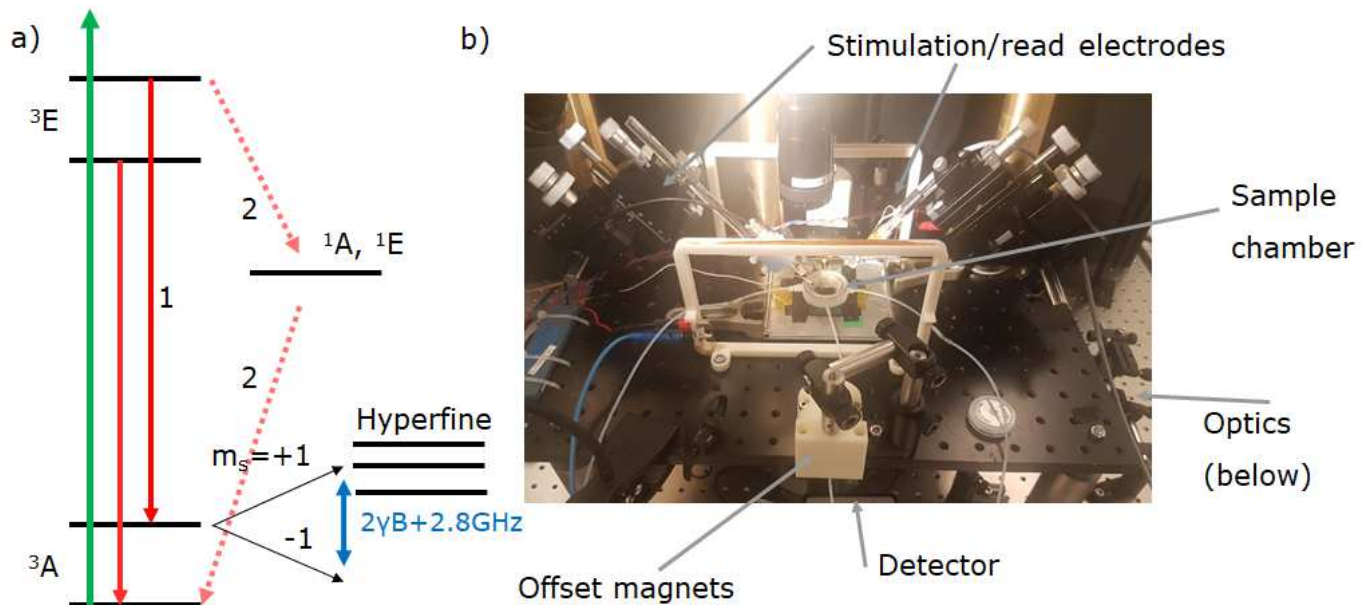


Figure 1: a) Simplified level structure of an NV^- defect in diamond. Under 532nm green laser illumination and on microwave resonance between the fine (and hyperfine) split levels, decay back to the ^3A ground state can occur nonradiatively/via IR emission, resulting in magnetic field sensitive drop in fluorescence. b) Image of our electrophysiology microscopy-style setup, with illumination and light collection under a raised platform, with access from above by contacting electrodes and a white light microscope.

however poses difficulties if this region is not easily accessible, such as inside the brain, or where signals must be highly spatially resolved. An alternative approach is to measure the magnetic field produced when these signals propagate as electrical current. Existing techniques for this such as magnetoencephalography (MEG) or magnetocardiography (MCG) are limited by reliance on cryogen cooled superconducting quantum interference device (SQUID) systems, which are expensive, bulky and have poor spatial resolution[1].

A recently developed alternative is to sense magnetic fields using nitrogen vacancy (NV) centres in diamond[2]. Such defects, specifically the NV^- center, have an electronic structure that results in magnetic field dependent variation in fluorescence output under illumination with resonant microwaves (MW) and 532nm green laser light. This can be performed at room temperature, from DC to kHz+ bandwidth needed for ms-timescale biological signals and in close proximity (or even within[3]) cells or tissue, due to the excellent biocompatibility of diamond. The high density of such defects in the material also makes possible imaging of biological signals near the optical diffraction limit with micrometer scale resolution.

Figure 1,a) shows the simplified level structure of an NV^- defect in diamond used for such sensing. Excitation by a 532nm pump laser can decay in two ways. The most likely, labeled (1) is directly in the triplet state between ground ^3A and excited ^3E state. However, if microwaves are applied on resonance between the ^3A state and its fine (and

hyperfine) split levels (2.8GHz) followed by pump excitation, decay back to the ground state can occur through process (2), via singlet shelving states 1A , 1E and nonradiative processes/weak infrared emission peaking at 1042nm[4]. This leads to a drop in fluorescence output on microwave resonance of up to 30% for a single NV, or 1-2% for a large NV ensemble. This process is termed ODMR: optically detected magnetic resonance. The $m_s=\pm 1$ states can be Zeeman split by a magnetic field, which shifts the resonance frequency, allowing detection of the field amplitude by monitoring fluorescence output. The relation between field and resonance shift is given by $2\gamma B=28\text{Hz/nT}$ and shifts down to a few Hz can be detected within one second of acquisition time, corresponding to the nano to picotesla level fields expected from biological signals.

3 Current State of the Art

The field of biosensing with NV magnetometry today can be broadly broken down into 3 subdivisions. The first is bulk magnetometry, with zero spatial resolution, collecting all emitted fluorescence from an NV ensemble and aiming for maximum overall sensitivity, limited by laser beam and/or diamond crystal size . The second is widefield imaging magnetometry, aiming for realtime imaging of magnetic field at high resolution using a microscope objective. The third is scanning magnetometry, using a confocal setup and nanodiamonds either on a scanning tip or in the sample. This work will focus on the first 2 aspects, while a recent review of the 3rd is given by Schirhagl et al. [5]. An excellent up to date summary of the field in general is given in the recent preprint by Barry et al.[6].

A key work in the field of bulk magnetometry biosensing is the detection of single neuron action potentials primarily from a marine worm by Barry et al.[7], with excellent $15\text{pT}/\sqrt{Hz}$ low frequency sensitivity. Few groups have yet to replicate this level of sensitivity, let alone on a biological specimen. Full vector magnetometry has recently been demonstrated by the same group with $50\text{pT}/\sqrt{Hz}$ sensitivity[8]. When considering the literature, a distinction must be drawn between DC-low frequency sensitivity and the typically significantly better AC ($>10\text{KHz}$) sensitivity that can be several orders of magnitude better by using pulsed dynamical decoupling techniques. Work by Hall et al.[9], Wolf et al.[10] and Masuyama et al.[11] have shown AC sensitivity of better than $10\text{pT}/\sqrt{Hz}$ using these methods. These frequencies are however far too high for detection of many biological signals in the sub-kHz regime. The best reported low frequency/DC sensitivities are typically worse, such as the works by Zheng et al.[12, 13] or by Clevenson et al. [14] with $\text{few-nT}/\sqrt{Hz}$, in a vector configuration by by Zhao et al.[15] with $5\text{nT}/\sqrt{Hz}$. Recent novel approaches promise improved sensitivities in this low frequency regime, such as the work by Chatzidrosos et al.[16] using an optical cavity to achieve $28\text{pT}/\sqrt{Hz}$ or the very recent work by Fescenko et al.[17] promising $\text{sub-pT}/\sqrt{Hz}$ sensitivity using flux concentrators. Novel techniques such as laser threshold magnetometry

[18, 19] using optical absorption promise further improvement in bulk sensitivity. There has also been important parallel effort in constructing integrated miniaturised sensors such as the work with CMOS by Ibrahim et al.[20] showing $250\text{nT}/\sqrt{Hz}$ sensitivity, Kim et al.[21] and by Sturmer et al.[22]. Such sensors may one day be extremely useful in a clinical diagnostic setting, but require further sensitivity improvement.

For widefield imaging, a primary goal is to image the field from biological signals (such as neuron action potentials)[23, 24]. However, sensitivities are typically on the $250\text{nT}-2\mu\text{T}/\sqrt{Hz}$ level, as yet insufficient for imaging pT-level fields[25]. Biosensing imaging work has therefore focused on samples which have a strong magnetic field due to the presence of ferromagnetic material, such as the work by Le Sage et al.[26] on magnetotactic bacteria or by Glenn et al. [27] and Davis et al.[28] with cells labeled with magnetic material (Fe). Several works have studied magnetic microbeads, the tracking of which can have applications in biological study[29]. The majority of work however has focused on imaging non-biological samples with far stronger magnetic fields, such as work on geological samples by Glenn et al.[30], vortices in superconductors by Schlusell et al.[31], ferromagnetic nanowires by Lee et al.[32] and electrical circuits by Horsley et al.[33]. Several works have also focused on imaging the properties of the diamond, such as imaging diamond stress by Kehayias et al.[34] and the properties of nanopillar arrays patterned into the diamond by McCloskey et al.[35]. Further progress in widefield imaging sensitivity is difficult since many of the improvements suggested for low frequency sensing may not be readily applicable to field imaging.

4 Typical Setup

The most typical NV magnetometer setup as pictured in Figure 1,b) is the inverted microscope geometry, where laser excitation and light collection is performed with the diamond held on a raised platform. Such a configuration has developed from typical electrophysiology microscopy setups. This allows a test sample to be placed above and in contact with the diamond, with easy access to it and a sample from above for placement of a white light microscope, stimulating electrodes or other necessary equipment. Both pump light and fluorescence collection may take place through the same lens - commonly either an aspheric condenser or a microscope objective - using a dichroic mirror and optical filter to split the red/green components. Alternatively, the pump laser may be directed separately onto the diamond, either perpendicular to the diamond surface or at Brewster's angle for diamond (67.5 degrees) to maximise coupling into the diamond. Such a lab bench configuration is not easily adapted for field sensing from living specimens in a clinical setting. We have recently demonstrated that magnetometry can be performed in a more flexible handheld setup, with pump laser fibre coupled into a box containing required optics and electronic components, more practical for diagnostic purposes[36].

5 Sensing Challenges

5.1 Fundamental Limits

The fundamental limit for sensing with an NV centre ensemble is defined by two main aspects: shot noise from the strong fluorescence background originating from transition directly from excited to ground triplet state and the low 1-3% change in fluorescence level on microwave resonance. This is the difficult task of detection of a small dip in brightness on a large bright background with a consequently high shot noise level. This shot noise limited regime means sensitivity improves with the square root of NV number (larger ensemble) and by high pump laser power (up to the order of Watts). Such power must be delivered at a wavelength shorter than the optical gap within the defect (637nm), but not so short as the energy gap from the defect to the conduction band ($\approx 450\text{nm}$) in order to remain within the defect state. The majority of diamond NV experiments in the literature use 532nm diode pumped solid state (DPSS) lasers, where cost and availability impose a practical limit of 2-5W on pump power. In diamonds available today with NV center densities in the parts per billion-low parts per million range, this can produce red fluorescence output from a planar diamond surface in the 1-50mW range. The majority of the fluorescence produced is trapped within the diamond by its high refractive index.

In practice, reaching this shot noise limited regime is difficult due to laser technical noise and electrical readout noise. Technical noise can be eliminated through common mode rejection using a balanced photodetector or by sampling the input laser beam and digitally subtracting it from the fluorescence signal[8]. Electrical readout noise originates primarily from the amplifiers used but also from the choice of photodiode - whereas a larger diode can collect more fluorescence, higher capacitance can increase noise and limit bandwidth.

5.2 Diamond Material

Sensitivity is defined by two properties that depend on the diamond material structure: contrast, the dip in fluorescence output on microwave resonance and resonance linewidth, proportional to the dephasing time T_2^* [38]. Contrast is typically worse for a larger ensemble of NV centres (1-3%) than a single isolated NV centre (10-30%). These features can be significantly improved through careful selection of exposure dose, through ^{12}C isotopic purification[39], through understanding the role of strain[40] and by using pulsed microwave and readout schemes such as the Ramsey sequence or spin echo that reduce power broadening effects[2, 41]. Choice of CVD overgrowth and/or high pressure high temperature (HPHT) diamond combined with irradiation method is also important. Figure 2 shows ODMR for a ^{12}C purified sample. Typical purified linewidth FWHM is on the order of 1MHz, 10-50MHz for high density and unpurified samples.

Peak sensitivity is a tradeoff between high NV number (high brightness) and narrow ODMR linewidth. Brighter samples with higher NV density tend to have a broader linewidth and those with narrow linewidths tend to be low in brightness. The best diamonds currently available in literature have linewidths of the order of 1MHz, contrast of 1-2% at maximum field sensitivity and total fluorescence collection of 30-40mW at 3-5W of pump power, with a simple estimate based on realistic collection efficiencies giving a shot noise limited sensitivity to DC and low frequency fields on the order of 10-20pT/ \sqrt{Hz} .

5.3 Laser coupling and light collection

A factor critical to good performance in diamond NV magnetometry is coupling laser light in at the Brewster angle for diamond. This produces significant improvements in fluorescence generation by both coupling more pump light into the diamond and increasing internal reflection of the pump light, illuminating more NV centres[42]. This also has the additional benefit of minimising damaging pump laser leakage into any biological sample. Directing the pump light through a highly focused microscope objective, perpendicular to the sample can lead to saturation in the ODMR amplitude and reduction in contrast and sensitivity at higher power. Such an objective placement can still be used for fluorescence collection. Care must be taken using a Brewster's angle configuration to correctly polarise the incident light e.g. by using a polarising beamsplitter and half wave plate combination. It also is possible to utilise more than one laser beam incident on the diamond at the correct angle and sample both beam into the reference of a balanced photodetector while rejecting the technical noise of both. This permits using 2 cheaper DPSS 1-2W lasers in combination to achieve greater sensitivity. For imaging, collection efficiency will be limited by the numerical aperture of the objective. For bulk magnetometry, use of an aspheric condenser lens (ideally antireflective coated) can maximise fluorescence collection.

5.4 Magnetic Noise

In any practical laboratory or clinical setting, there will be substantial magnetic field generation from mains transformers in equipment and in building wiring. This occurs primarily at the fundamental mains frequency (European 50Hz or North American 60Hz) and the 3rd harmonic (150 or 180Hz) arising from magnetic hysteresis in the transformer, but also at higher harmonics and likely at multiples of 3 phase frequencies. Such low frequency fields are difficult to shield against, requiring full mu-metal enclosure, impractical for processing of biological samples, or extremely costly fully shielded rooms into which feeding piping or cabling is equally hard. Active cancellation, by using field coils to generate a counter field to the noise, can reduce it but this is hard to achieve for multi-axis

sensing at a small 1-2mm diamond, at kHz bandwidth and operating at $\text{sub-nT}/\sqrt{Hz}$ sensitivity. The majority of commercially available systems cannot achieve these levels of field cancellation.

As an alternative, the magnetically sensitive signal from the diamond magnetometer can be processed and filtered by Fast Fourier Transform (FFT) methods. This requires not only effective filtering but minimal filtering, since many biological signals have frequency components in the 10-500Hz range and any strong filtering here will distort or remove the desired signal entirely. Such a filter must adapt to any drift in mains frequency and be able to capture any transient noise (such as from a fan or pump turning on and off). Further, it must counter phase drift in the mains supply, which acts to spread the mains noise across a wider frequency range.

In Figure 3 we demonstrate how effective this can be. Data is collected for 60sec in order to give good frequency discrimination. Low frequency and DC drift arising from laser power fluctuations is first removed by a highpass filter at 10Hz. Next, a 50Hz zero phase pure sine wave is correlated with a readout of the fundamental mains frequency obtained from tapping input to a transformer, in order to obtain a time series of the phase drift over the measurement period. A slight constant phase shift can be added to this signal to account for any phase shift due to inductive effects, then normalised and subtracted from the magnetic readout. This process can be repeated several times to remove multiple (additive) sources of noise with different phase. It can then be repeated at 150Hz, 250Hz or other strong harmonics of mains. Consequently, the phase drift broadening is removed in the frequency domain. Narrow notch or bandstop filters can then be used, centered on the noise frequencies, to remove any remaining noise components (Figure 3,c) . Any high frequency RF noise can then be removed by a final lowpass filter at 5-10kHz. The overall effect in the data is a reduction in noise by orders of magnitude, down to the electrical and optical noise floors (inset, Figure 3,b).

5.5 Laser Heating

In order to maximise sensitivity in NV centre experiments limited by fluorescence shot noise, high laser powers of the order of several Watts are required. This presents a challenge of focusing a high power visible laser beam onto a mm-size diamond while remaining within the $\leq 37^{\circ}\text{C}$ range from most biological processes. Sudden changes in temperature, such as from fast ramping of the laser to high power, can also cause problems. Heat must be dissipated from the diamond while minimising the distance between diamond and sample, to maximise biological signal magnetic field strength at the diamond. Samples often cannot be placed directly on a metal heatsink, as this would short out any conduction paths and potentially interfere with the microwave or DC magnetic offset fields.

Figure 4 shows the effect of slow ramping the laser power on the electrical readout on

the local field potential evoked in the CA1 region of the hippocampus in a slice preparation of a mouse brain. By using a metal foil layer as heatsink and thinner Kapton tape as electrical insulation, higher power can be reached with the signal strength improving through gradual heating. We observed no signal for direct slice transfer to a diamond preheated by the laser at 1 or 2W, attributable to thermal shock on placing it on the warm diamond.

One additional way of achieving good thermal dissipation is to have the diamond in contact with a SiC wafer[43]. Another method we utilise is to use plates of aluminium nitride (AlN) with a laser cut hole for the diamond. AlN is cheaper to purchase, easier to machine and has a good thermal conductivity while being an electrical insulator. Thermal effects on the magnetometry can be canceled by driving two $m_s = \pm 1$ hyperfine transitions, although at a factor 2x cost in sensitivity[44].

5.6 Measurement Environment

In order to maintain optimum sensitivity, the measurement environment in proximity to the diamond must be well controlled. This is difficult to achieve in practice due to the need to hold biological samples in solution than can vary in volume or composition over time, due to movement (particularly muscle tissue) and due to changes in temperature, all of which can act to shift the optimum microwave frequency and power required to maximise magnetometer sensitivity.

The efficiency of microwave coupling to the diamond can be considerably affected by having a water or other solution in close proximity. This is particularly critical for antennas with a narrow resonance, such as wire loops. To counter this, a broadband antenna fabricated on a PCB board can be used followed by reoptimisation of MW power (often by several orders of magnitude) after an acceptable stable solution level is reached. In order to maintain sensitivity, it is critical to keep a constant solution level and constant flow, whereby shifts in the MW resonance are avoided. Sample movement can also produce such resonance shifts: if necessary, muscle inhibitors such as butanedione monoxime (BDM) (dissected tissue) or local anesthetic (living specimen) can be introduced to counter such effects.

Another factor is gradual thermal drift, caused by microwave or - as previously discussed - laser heating. Thermal drift can, over the course of minutes, push the optimum microwave resonance frequency away from the setpoint frequency, reducing sensitivity. An ODMR sweep can be performed after every few measurements in order to reoptimise. Alternatively, a low frequency signal can be applied to a test coil aligned with the offset field and maximised in a FFT of a short period readout.

A further key factor is minimising distance from the diamond. Since magnetic field strength drops as the cube of the distance, only a small difference in separation (order of

μm [25]) can make a significant difference in detection. This poses particular challenges for biological systems, where the tissue generating the signal may unavoidably be many millimetres from the sample (such as within muscle or under bone). In a microscopy setup, in Ringer's solution, tissue samples can partially float from the surface. Using a Pt and nylon harp can help this without disrupting the offset field significantly. Using hooks and electrodes to hold the sample onto the diamond can also be effective, although care must be taken not to damage the tissue.

5.7 Stimulating Electrode Type and Design

Diamond magnetometry requires a mT scale DC offset field in order to split the defect levels and obtain good contrast and sensitivity. In electrophysiology experiments only the electrical performance of the test electrodes is important and no offset magnetic field is required. This means many types of electrical stimulation electrodes that can be purchased contain some steel, often in the outer sheath of concentric-type stimulation electrodes. This leads to such electrodes becoming magnetised in the DC offset field, which disrupts the field close to the diamond and significantly reduces magnetic sensitivity. An alternative is to use Pt/Ir electrodes with a glass or plastic outer sheath, or to fabricate similar electrodes from biocompatible Ti or W wire (Cu is often not suitable unless coated with Au or Ag/AgCl).

5.8 Camera Limitations

The camera limitations of NV centre widefield fluorescence imaging are discussed in detail in the recent work by Wojciechowski et al.[44]. A key problem with NV ensemble widefield imaging is bit depth. The majority of digital cameras in general and used for microscopy work in only 8 or 10 bit depth (since the human eye cannot distinguish a greater color or monochrome palette). With a large background fluorescence brightness, this can result in the on MW resonance contrast being spread across too few digitisation levels. Specialist 12 and 16 bit cameras can be purchased, as can those with initial analog black level correction, that can spread the contrast across the full digitisation range.

Such a high level of background brightness means shot noise will significantly exceed readout noise or dark noise on each pixel. This shot noise background severely restricts imaging sensitivity - using a detection area of $5 \times 5 \text{mm}$ with $3.5 \mu\text{m}$ square pixel size (approximately 2 Mpixels) and isotopically purified diamonds with a linewidth of 1MHz, contrast of 2% and collecting a fluorescence output of $\approx 30 \text{mW}$, the per pixel shot noise limited sensitivity of an imaging system is approximately $10 \text{nT}/\sqrt{\text{Hz}}$. This presently restricts imaging of biological signals to specific, low bandwidth cases rather than imaging of pT-level signals such as those from neural activity.

Another issue is imaging of artifacts that can easily resemble magnetic fields. A selection of these are highlighted in Figure 5. Variation in microwave power and resonance frequency across the image width can be more significant than the shift resulting from local changes in magnetic field (Figure 5,a), which can in turn be mistaken for localised magnetic field imaging. Jitter or wobble in repeated averaged images can produce patterns that appear to be localised to electrodes or areas where a field is expected (Fig 5,b) In addition, low frequency vibration of the diamond itself in the typical frequency range of biological signals can be observed in a magnetic-field like pattern of fluorescence brightness change (Fig 5,c). Finally, magnetic field-resembling diffraction patterns can arise from imperfect interfaces and air or solution gaps between diamond and sample.

5.9 Averaging

One way to improve sensitivity is to repeat the signal N thousands of times and then average, with improvement proportional to \sqrt{N} . This however places considerable demands on a biological sample, for example due to fatigue in a muscle, due to damage induced in the tissue by repeated stimulation or due to thermal degradation. It is possible for a sample to survive for substantial time (order of hours) if heat and oxygen levels are kept favourable, with the sample held in a carbogenated (5% carbon dioxide, 95% oxygen) solution.

6 Future Prospects

Substantial effort in recent years has gone into developing pulsed laser/microwave schemes for field detection and imaging. These have been very successful in improving sensitivity to high frequency AC fields ($>10\text{kHz}$) via dynamical decoupling methods, rather than in the limit of low frequency and DC signals. A significant problem for DC sensing is the time required to read a large ensemble of NV centres, on the order of $150\mu\text{s}$ such as in the work by Wolf et al.[10] and up to milliseconds in our own measurements with a larger ensemble which we show in Figure 6. This can limit the measurement bandwidth to below that required for many biological sensing applications. A prospect to enhance sensitivity in the pulsed regime may be microwave pulse shaping, using an arbitrary waveform generator and optimal control methods to boost readout fidelity[45].

An alternative to fluorescence imaging is to instead monitor the absorption of green or infrared light through the diamond. This technique has demonstrated better than $100\text{nT}/\sqrt{Hz}$ sensitivities in an optical cavity configuration[46]. Recent work has focused on using this absorption to control the lasing threshold in order to boost the level of contrast observed[19, 18]. Such laser threshold experiments can potentially work with other materials beyond diamond. Absorption may also be exploited using interferometry

techniques, placing the diamond with the sample in one arm of a Mach-Zehnder configuration and detecting magnetic field through the effect of the field-dependent absorption of the diamond on the interference pattern generated at the output. This requires minimising reflective losses and good stable transmission through the diamond in order to be realised.

Finally, it is hoped that advances in diamond material processing may drive future development. In particular, improvements in CVD growth, nitrogen levels and conversion to NV^- centres, optimisation of irradiation and dealing with material strain. Patterning of the diamond may allow a greater fraction of the fluorescence to escape, boosting efficiency[47].

7 Conclusion

Sensing of biological signals via their magnetic fields using diamond NV centers provides a potential route to better measure and understand them, whether in an electrophysiology-style microscopy configuration or from MEG-style sensing of inaccessible tissues in a living subject. Previous work has shown the technique to be biocompatible and widely applicable to a number of different systems, in both a bulk sensing and imaging configuration. There are, however, challenges in realising such measurements, both in general from material limitations and the need to filter out unwanted noise, to specific demands unique to biosensing, such as maintaining temperature stability. In the coming years, further advances in sensitivity are required in order to realise ambitious sensing goals. A number of promising ideas are currently under development, particularly using pulsed schemes and in improving diamond material quality.

Conflict of Interest Statement

The authors declare that the research was conducted in the absence of any commercial or financial relationships that could be construed as a potential conflict of interest.

Author Contributions

JLW, NWH and LT performed experiments for which data is shown as figures in this work. JLW wrote the manuscript with input from AH, KBS, ULA, JFMP and NWH.

Funding

The work presented here was funded by the Novo Nordisk foundation through the synergy grant bioQ and the bigQ Center funded by the Danish National Research Foundation (DNRF).

Acknowledgments

We acknowledge the assistance of Kristian Hagsted Rasmussen for fabrication and diamond processing and Axel Thielscher, Mursel Karadas (current and former DTU Heath Tech) and Adam Wojciechowski (former DTU Physics, currently Jagiellonian University, Krakow) for contributions and prior experimental and theoretical modeling work.

References

- [1] E. Boto, N. Holmes, J. Leggett, G. Roberts, V. Shah, S. S. Meyer, L. D. Muñoz, K. J. Mullinger, T. M. Tierney, S. Bestmann, et al., *Nature* **555**, 657 (2018), URL <https://doi.org/10.1038/nature26147>.
- [2] J. M. Taylor, P. Cappellaro, L. Childress, L. Jiang, D. Budker, P. R. Hemmer, A. Yacoby, R. Walsworth, and M. D. Lukin, *Nature Physics* **4**, 810 (2008), URL <https://doi.org/10.1038/nphys1075>.
- [3] L. P. McGuinness, Y. Yan, A. Stacey, D. A. Simpson, L. T. Hall, D. Maclaurin, S. Praver, P. Mulvaney, J. Wrachtrup, F. Caruso, et al., *Nature Nanotechnology* **6**, 358 (2011), URL <https://doi.org/10.1038/nnano.2011.64>.
- [4] V. M. Acosta, A. Jarmola, E. Bauch, and D. Budker, *Physical Review B* **82** (2010), URL <https://doi.org/10.1103/physrevb.82.201202>.
- [5] R. Schirhagl, K. Chang, M. Loretz, and C. L. Degen, *Annual Review of Physical Chemistry* **65**, 83 (2014), URL <https://doi.org/10.1146/annurev-physchem-040513-103659>.
- [6] J. F. Barry, J. M. Schloss, E. Bauch, M. J. Turner, C. A. Hart, L. M. Pham, and R. L. Walsworth, *arXiv* (2019).
- [7] J. F. Barry, M. J. Turner, J. M. Schloss, D. R. Glenn, Y. Song, M. D. Lukin, H. Park, and R. L. Walsworth, *Proceedings of the National Academy of Sciences* **113**, 14133 (2016), ISSN 0027-8424, <https://www.pnas.org/content/113/49/14133.full.pdf>, URL <https://www.pnas.org/content/113/49/14133>.

- [8] J. M. Schloss, J. F. Barry, M. J. Turner, and R. L. Walsworth, *Physical Review Applied* **10** (2018), URL <https://doi.org/10.1103/physrevapplied.10.034044>.
- [9] L. T. Hall, C. D. Hill, J. H. Cole, and L. C. L. Hollenberg, *Physical Review B* **82** (2010), URL <https://doi.org/10.1103/physrevb.82.045208>.
- [10] T. Wolf, P. Neumann, K. Nakamura, H. Sumiya, T. Ohshima, J. Isoya, and J. Wrachtrup, *Physical Review X* **5** (2015), URL <https://doi.org/10.1103/physrevx.5.041001>.
- [11] Y. Masuyama, K. Mizuno, H. Ozawa, H. Ishiwata, Y. Hatano, T. Ohshima, T. Iwasaki, and M. Hatano, *Review of Scientific Instruments* **89**, 125007 (2018), URL <https://doi.org/10.1063/1.5047078>.
- [12] H. Zheng, J. Xu, G. Z. Iwata, T. Lenz, J. Michl, B. Yavkin, K. Nakamura, H. Sumiya, T. Ohshima, J. Isoya, et al., *Physical Review Applied* **11** (2019), URL <https://doi.org/10.1103/physrevapplied.11.064068>.
- [13] H. Zheng, Z. Sun, G. Chatzidrosos, C. Zhang, K. Nakamura, H. Sumiya, T. Ohshima, J. Isoya, A. W. Jorg Wrachtrup, and D. Budker, *arXiv* (2019).
- [14] H. Clevenston, M. E. Trusheim, C. Teale, T. Schröder, D. Braje, and D. Englund, *Nature Physics* **11**, 393 (2015), URL <https://doi.org/10.1038/nphys3291>.
- [15] B. Zhao, H. Guo, R. Zhao, F. Du, Z. Li, L. Wang, D. Wu, Y. Chen, J. Tang, and J. Liu, *IEEE Magnetics Letters* **10**, 1 (2019), URL <https://doi.org/10.1109/lmag.2019.2891616>.
- [16] G. Chatzidrosos, A. Wickenbrock, L. Bougas, N. Leefer, T. Wu, K. Jensen, Y. Dumeige, and D. Budker, *Physical Review Applied* **8** (2017), URL <https://doi.org/10.1103/physrevapplied.8.044019>.
- [17] I. Fescenko, A. Jarmola, I. Savukov, P. Kehayias, J. Smits, J. Damron, N. Ristoff, N. Mosavian, and V. M. Acosta, *arXiv* (2019).
- [18] J. Jeske, J. H. Cole, and A. D. Greentree, *New Journal of Physics* **18**, 013015 (2016), URL <https://doi.org/10.1088/1367-2630/18/1/013015>.
- [19] Y. Dumeige, J.-F. Roch, F. Bretenaker, T. Debuisschert, V. Acosta, C. Becher, G. Chatzidrosos, A. Wickenbrock, L. Bougas, A. Wilzewski, et al., *Optics Express* **27**, 1706 (2019), URL <https://doi.org/10.1364/oe.27.001706>.
- [20] M. I. Ibrahim, C. Foy, D. R. Englund, and R. Han, in *2019 IEEE International Solid-State Circuits Conference - (ISSCC)* (IEEE, 2019), URL <https://doi.org/10.1109/isscc.2019.8662434>.

- [21] D. Kim, M. I. Ibrahim, C. Foy, M. E. Trusheim, R. Han, and D. R. Englund, *Nature Electronics* **2**, 284 (2019), URL <https://doi.org/10.1038/s41928-019-0275-5>.
- [22] F. M. Stürner, A. Brenneis, J. Kassel, U. Wostradowski, R. Rölver, T. Fuchs, K. Nakamura, H. Sumiya, S. Onoda, J. Isoya, et al., *Diamond and Related Materials* **93**, 59 (2019), URL <https://doi.org/10.1016/j.diamond.2019.01.008>.
- [23] L. T. Hall, G. C. G. Beart, E. A. Thomas, D. A. Simpson, L. P. McGuinness, J. H. Cole, J. H. Manton, R. E. Scholten, F. Jelezko, J. Wrachtrup, et al., *Scientific Reports* **2** (2012), URL <https://doi.org/10.1038/srep00401>.
- [24] L. Hall, D. Simpson, and L. Hollenberg, *MRS Bulletin* **38**, 162 (2013), URL <https://doi.org/10.1557/mrs.2013.24>.
- [25] M. Karadas, A. M. Wojciechowski, A. Huck, N. O. Dalby, U. L. Andersen, and A. Thielscher, *Scientific Reports* **8** (2018), URL <https://doi.org/10.1038/s41598-018-22793-w>.
- [26] D. L. Sage, K. Arai, D. R. Glenn, S. J. DeVience, L. M. Pham, L. Rahn-Lee, M. D. Lukin, A. Yacoby, A. Komeili, and R. L. Walsworth, *Nature* **496**, 486 (2013), URL <https://doi.org/10.1038/nature12072>.
- [27] D. R. Glenn, K. Lee, H. Park, R. Weissleder, A. Yacoby, M. D. Lukin, H. Lee, R. L. Walsworth, and C. B. Connolly, *Nature Methods* **12**, 736 (2015), URL <https://doi.org/10.1038/nmeth.3449>.
- [28] H. C. Davis, P. Ramesh, A. Bhatnagar, A. Lee-Gosselin, J. F. Barry, D. R. Glenn, R. L. Walsworth, and M. G. Shapiro, *Nature Communications* **9** (2018), URL <https://doi.org/10.1038/s41467-017-02471-7>.
- [29] Z. Kazi, I. Shelby, N. Brunelle, H. Watanabe, K. M. Itoh, P. Wiggins, and K.-M. Fu, in *Conference on Lasers and Electro-Optics* (OSA, 2019), URL https://doi.org/10.1364/cleo_at.2019.am4i.1.
- [30] D. R. Glenn, R. R. Fu, P. Kehayias, D. L. Sage, E. A. Lima, B. P. Weiss, and R. L. Walsworth, *Geochemistry, Geophysics, Geosystems* **18**, 3254 (2017), URL <https://doi.org/10.1002/2017gc006946>.
- [31] Y. Schlüssel, T. Lenz, D. Rohner, Y. Bar-Haim, L. Bougas, D. Groswasser, M. Kieschnick, E. Rozenberg, L. Thiel, A. Waxman, et al., *Physical Review Applied* **10** (2018), URL <https://doi.org/10.1103/physrevapplied.10.034032>.
- [32] M. Lee, B. Jang, J. Yoon, M. C. Mathpal, Y. Lee, C. Kim, S. Pane, B. J. Nelson, and D. Lee, *Nanotechnology* **29**, 405502 (2018), URL <https://doi.org/10.1088/1361-6528/aad2fe>.

- [33] A. Horsley, P. Appel, J. Wolters, J. Achard, A. Tallaire, P. Maletinsky, and P. Treutlein, *Physical Review Applied* **10** (2018), URL <https://doi.org/10.1103/physrevapplied.10.044039>.
- [34] P. Kehayias, M. J. Turner, R. Trubko, J. M. Schloss, C. A. Hart, M. Wesson, D. R. Glenn, and R. L. Walsworth, *Physical Review B* **100** (2019), URL <https://doi.org/10.1103/physrevb.100.174103>.
- [35] D. J. McCloskey, N. Dontschuk, D. A. Broadway, A. Nadarajah, A. Stacey, J.-P. Tetienne, L. C. L. Hollenberg, S. Prawer, and D. A. Simpson, *arXiv* (2019).
- [36] J. L. Webb, J. D. Clement, L. Troise, S. Ahmadi, G. J. Johansen, A. Huck, and U. L. Andersen, *Applied Physics Letters* **114**, 231103 (2019), URL <https://doi.org/10.1063/1.5095241>.
- [37] H. A. R. El-Ella, S. Ahmadi, A. M. Wojciechowski, A. Huck, and U. L. Andersen, *Optics Express* **25**, 14809 (2017), URL <https://doi.org/10.1364/oe.25.014809>.
- [38] E. Bauch, C. A. Hart, J. M. Schloss, M. J. Turner, J. F. Barry, P. Kehayias, S. Singh, and R. L. Walsworth, *Physical Review X* **8** (2018), URL <https://doi.org/10.1103/physrevx.8.031025>.
- [39] K. D. Jahnke, B. Naydenov, T. Teraji, S. Koizumi, T. Umeda, J. Isoya, and F. Jelezko, *Applied Physics Letters* **101**, 012405 (2012), URL <https://doi.org/10.1063/1.4731778>.
- [40] M. E. Trusheim and D. Englund, *New Journal of Physics* **18**, 123023 (2016), URL <https://doi.org/10.1088/1367-2630/aa5040>.
- [41] L. Rondin, J.-P. Tetienne, T. Hingant, J.-F. Roch, P. Maletinsky, and V. Jacques, *Reports on Progress in Physics* **77**, 056503 (2014), URL <https://doi.org/10.1088/0034-4885/77/5/056503>.
- [42] L. Bougas, A. Wilzewski, Y. Dumeige, D. Antypas, T. Wu, A. Wickenbrock, E. Bourgeois, M. Nesladek, H. Clevenson, D. Braje, et al., *Micromachines* **9**, 276 (2018), URL <https://doi.org/10.3390/mi9060276>.
- [43] J. F. Barry, M. J. Turner, J. M. Schloss, D. R. Glenn, Y. Song, M. D. Lukin, H. Park, and R. L. Walsworth, *Proceedings of the National Academy of Sciences* **113**, 14133 (2016), URL <https://doi.org/10.1073/pnas.1601513113>.
- [44] A. M. Wojciechowski, M. Karadas, C. Osterkamp, S. Jankuhn, J. Meijer, F. Jelezko, A. Huck, and U. L. Andersen, *Applied Physics Letters* **113**, 013502 (2018), URL <https://doi.org/10.1063/1.5026678>.

- [45] T. Nöbauer, A. Angerer, B. Bartels, M. Trupke, S. Rotter, J. Schmiedmayer, F. Mintert, and J. Majer, *Physical Review Letters* **115** (2015), URL <https://doi.org/10.1103/physrevlett.115.190801>.
- [46] S. Ahmadi, H. A. R. El-Ella, A. M. Wojciechowski, T. Gehring, J. O. B. Hansen, A. Huck, and U. L. Andersen, *Physical Review B* **97** (2018), URL <https://doi.org/10.1103/physrevb.97.024105>.
- [47] T.-Y. Huang, R. R. Grote, S. A. Mann, D. A. Hopper, A. L. Exarhos, G. G. Lopez, G. R. Kaighn, E. C. Garnett, and L. C. Bassett, *Nature Communications* **10** (2019), URL <https://doi.org/10.1038/s41467-019-10238-5>.

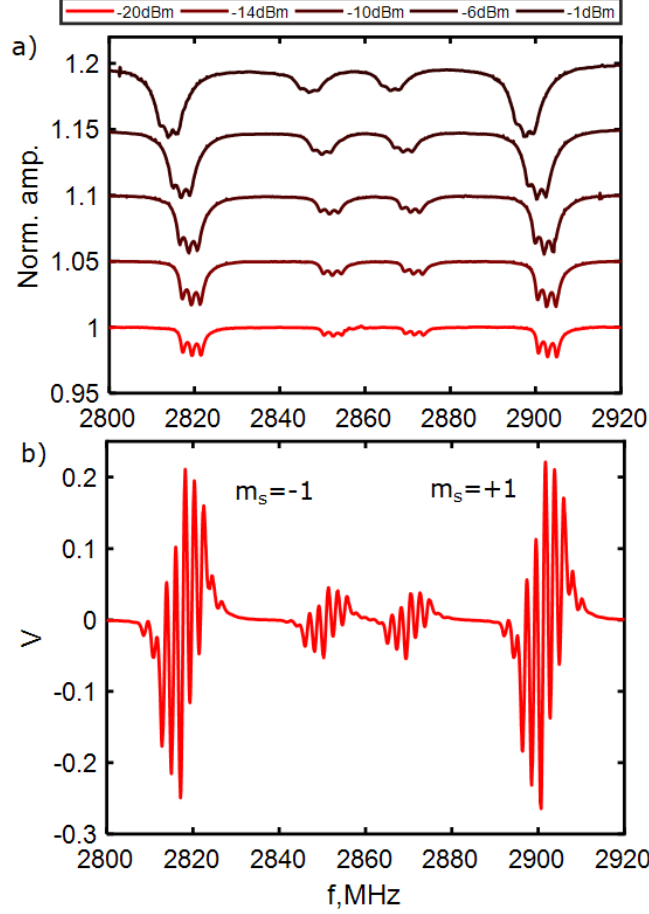


Figure 2: ODMR from our diamond sample. The ^{14}N diamond was ^{12}C enriched with $20\mu\text{m}$ of CVD overgrowth, then proton irradiated with N concentration $\approx 5\text{ppm}$. a) Normalised change in DC photovoltage with 2W pump power (max 6.5mW fluorescence) at a range of microwave input powers, each offset by 0.05. A $\approx 1.6\text{mT}$ offset field was applied with fine adjustment from field coils to overlap 2 NV axes and boost contrast to a maximum of 5.1%. Due to microwave broadening and resulting loss of the hyperfine features, actual peak sensitivity is reached at a lower 3.8% contrast. The downward frequency shift observed is due to heating by the microwave field. b) ODMR at peak sensitivity using a 33kHz MW frequency modulation of 500kHz mixed with a 2.16MHz hyperfine transition drive (see method details in the work by El-Ella et al.[37]). This boosts overall sensitivity to $100\text{pT}/\sqrt{\text{Hz}}$. Linewidth FWHM is approximately 1MHz.

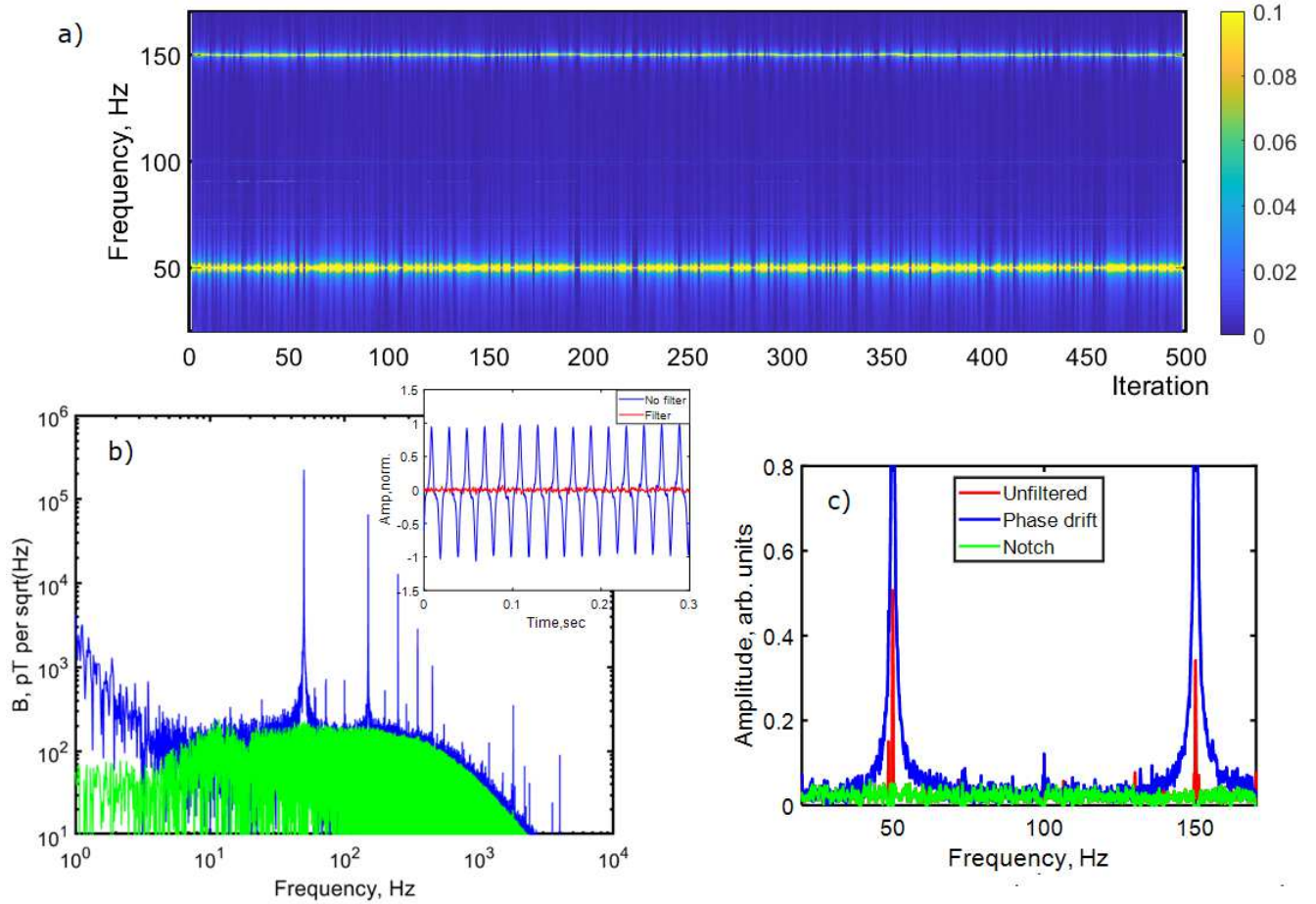


Figure 3: a) Normalised spectrogram of magnetometer pickup from 30-170Hz from FFT of successive 60sec long measurements (iterations) at regular intervals over a period of 8 hours. The variable phase drift during each measurement is seen as a broadening in frequency of the 50/150Hz mains noise peaks. b) Magnetometer sensitivity from a single 60sec measurement using 1W pump power while magnetically sensitive before and after filtering. The low frequency noise floor is approximately $150\text{-}200\text{pT}/\sqrt{\text{Hz}}$, (inset) timeseries of signal before and after filtering, showing significant improvement obtained, c) Single 60sec measurement before filtering (blue), after timeseries filtering (red) to remove phase drift and after notch filtering (yellow).

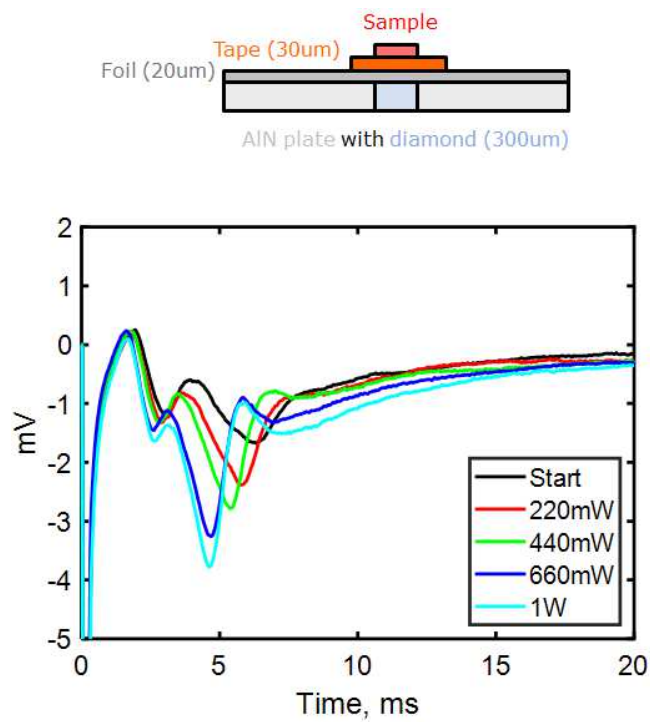


Figure 4: Change in mouse brain slice hippocampal field potentials recorded in the CA1 region at specific laser powers during laser ramp up (at 0.01W every 20s). Laser power was ramped to a maximum of 1W, with the slice thermally isolated from the diamond by a layer of $20\mu\text{m}$ thickness aluminium foil heatsunk into the surrounding solution and $30\mu\text{m}$ thickness Kapton tape. The diamond is within the center of a 2x2 cm AlN plate.

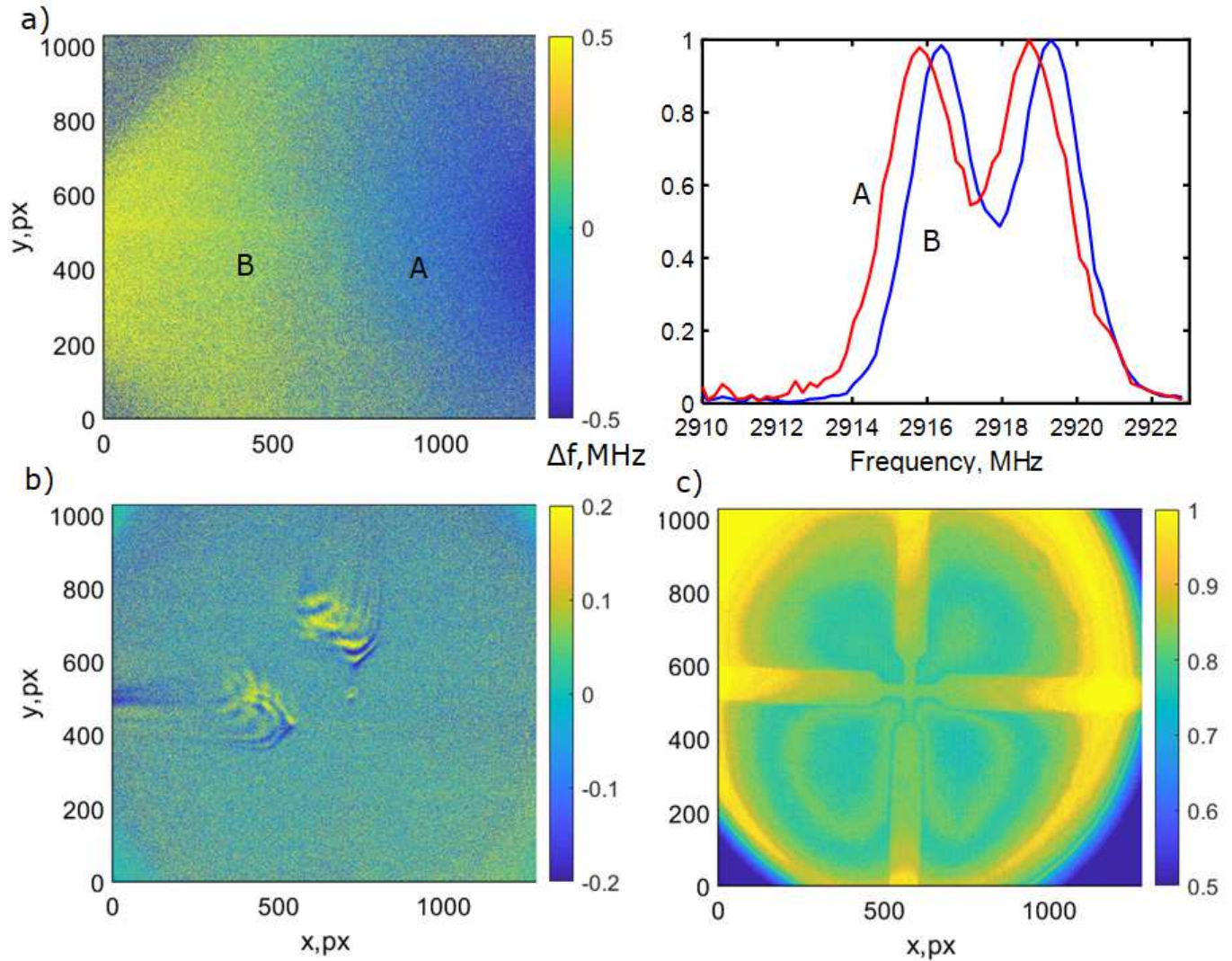


Figure 5: Artifacts in fluorescence imaging experiments of a Ti/Au 50nm cross on glass. In a) the variation of microwave field is shown across an image with a field of view (FOV) of approximately 1mm (using a x10 objective). The result is a difference in brightness at a given MW frequency that can resemble a field shift, as can be seen in the ODMR plot averaging a 200x200pixel region at different places (A,B) on the image. b) The effect of vibrations (image wobble) on averaging of 100 successive images taken at 1ms intervals using a 100x objective with $\approx 100\mu\text{m}$ FOV. c) Imaging at 7Hz of vibrational modes of the diamond itself, which appear as slight changes in brightness that can resemble magnetic field patterns.

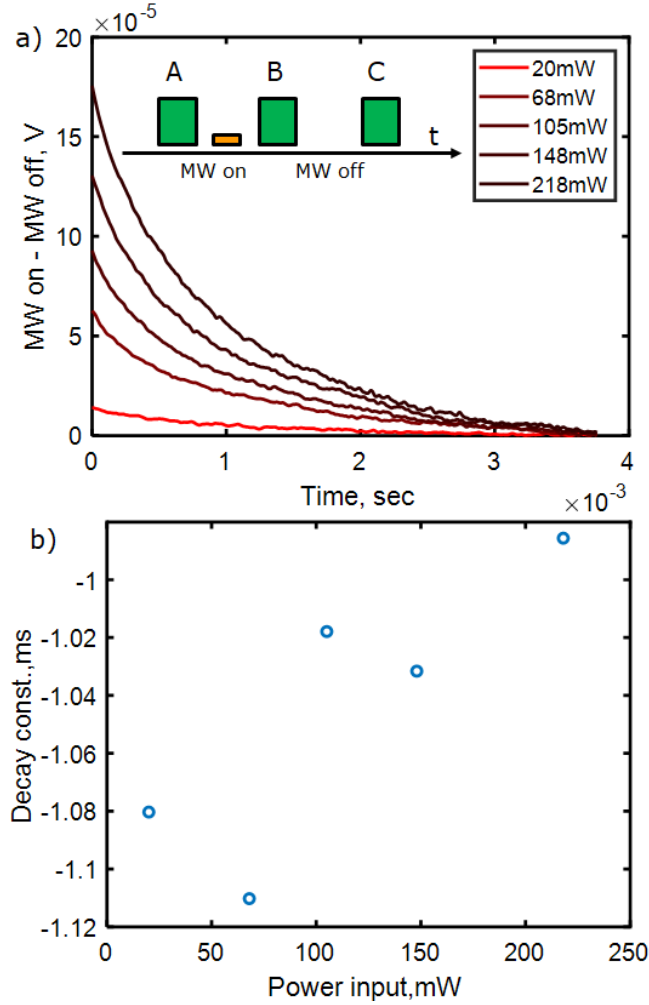


Figure 6: a) Subtraction of fluorescence photovoltage vs time from 2 pump laser pulses B,C of the same length (up to 4ms) as initialisation pulse A. Before B a 680ns π microwave pulse is applied (MW on) and before C, no MW pulse is applied (MW off). Times of up to 4ms are required to fully reset the ensemble back into the ground state (MW on-MW off=0). Data is taken at a range of pump laser powers from a Gaussian beam of waist $200\mu\text{m}$ incident at the Brewster angle on the sample detailed in the caption of Figure 2 . b) Fitting to an exponential, typical decay length was 1ms, reducing with higher pump power. This long readout time restricts field sensing bandwidth to 250Hz or 83Hz for a 3 pulse, common mode noise rejection scheme.